Lawrence Berkeley Laboratory
UNIVERSITY OF CALIFORNIA

Presented at the Third Adriatic Europhysics Study Conference on the Dynamics of Heavy-Ion Collisions, Hvar, Croatia, Yugoslavia, May 25-30, 1981

EXPERIMENTS WITH RELATIVISTIC HEAVY IONS: A POTPOURRI OF CHEMISTRY, CANIS MAJORIS AND GRAINS OF SILVER

Harry H. Heckman

May 1981

Prepared for the U.S. Department of Energy under Contract W-7405-ENG-48

LBL-12656

EXPERIMENTS WITH RELATIVISTIC HEAVY IONS: A POTPOURRI OF CHEMISTRY, CANIS MAJORIS AND GRAINS OF SILVER

Harry H. Heckman

Nuclear Science Division
Lawrence Berkeley Laboratory
University of California
Berkeley, CA 94720

This work was supported by the Director, Office of Energy Research, Division of Nuclear Physics of the Office of High Energy and Nuclear Physics of the U.S. Department of Energy under Contract W-7405-ENG-48.

LBL-12656

EXPERIMENTS WITH RELATIVISTIC HEAVY IONS: A POTPOURRI OF CHEMISTRY, CANIS MAJORIS AND GRAINS OF SILVER

Harry H. Heckman

Nuclear Science Division, Lawrence Berkeley Laboratory
University of California, Berkeley, CA 94720

Abstract: A selection of three experimental programs, unique in their applied techniques and physics objectives, form the basis of a review of contemporary experiments in relativistic heavy ion physics.

1. Introduction

The concatenation of innovative accelerator technology and scientific interest during the decade of the 1970s marks one of the most incisive periods in studies of relativistic heavy ion (RHI) physics. Within a span of a few years, the kinetic energies of accelerated nuclei available in the laboratory increased by more than three orders of magnitude. The physics of heavy ions has thus been literally propelled from energies in the realm of 0.01 A GeV to ~10 A GeV, creating new vistas and a powerful means to search for unexpected and, undoubtedly, new aspects of nuclear matter. As implied by my title, experiments in RHIs encompass a rich variety of techniques and infusion from a broad range of scientific disciplines. To pursue this thesis, I shall review three selected RHI experiments that represent, to me, uniquely different experimental approaches. Their similarity, however, is that they have produced striking and quite impressive results. The first experiments involve analytic radiochemistry studies of target fragmentation by protons and RHIs. The next section presents early experimental results from two-pion correlation experiments--experiments that utilize the Hanbury-Brown and Twiss effect first used 25 years ago to measure the stellar diameter of Canis Majoris A (Sirius). The third experiment is on the evidence for anomalous nuclei among the projectile fragments (PF) of relativistic nuclei. This is a nuclear emulsion experiment, hence entails track following along "grains of silver".

2. Target Fragmentation: Radiochemistry Studies and Associated Multiplicities

Because RHI physics can be considered to be an extension of high-energy particle physics (e.g., baryon numbers B = 0,1) to multi-baryon systems, it was logical that high energy concepts be introduced to RHI.[1-4] The fact is that some of the earliest experimental results to come from the Bevatron/ Bevalac on the fragmentation of relativistic nuclei[5] gave strong evidence that the hypotheses of limiting fragmentation[6-9] and the factorization of cross sections, pertinent to the description of single-particle inclusive spectra, were applicable to RHI. "Limiting fragmentation" means, in essence, that a distribution of products with finite energies in the target/projectile rest frames approaches a limiting form as the beam energy increases. "Factorization" in the region of limiting fragmentation infers that the modes of fragmentation of the target (projectile) are independent of the projectile (target) nucleus.

Over the past several years, there have been a variety of radiochemical experiments on the cross sections and recoil properties of target fragmentation products (radionuclides) formed by the reactions of RHI (and protons) with various target nuclei. Among the objectives of these experiments are to test the hypotheses of limiting fragmentation and factorization. The experiments

have proceeded with little fanfare or recognition, but have yielded important information on many aspects of the reaction mechanisms between nuclei at intermediate and relativistic energies.

Among the radiochemical experiments on target fragmentation I want to discuss are those by Cumming and co-workers,[10,11] who demonstrated the approach to limiting fragmentation by examining the energy dependence of the slope of the mass-yield curve, which is taken to be an approximate measure of the excitation energy transferred to the target nucleus from the bombarding particle; a smaller slope means a greater average mass loss, hence higher excitation energy, on the average. The mass yield curves presented in Fig. 1 give the production cross sections as a function of the product mass of the fragment residues from the fragmentation of Cu by 80-GeV ^{40}Ar, (ref. 10) 25-GeV ^{12}C and 28-GeV ^{1}H (ref. 11). At these beam energies the striking feature of the mass yields is that they are essentially the same except for magnitude, which scales as σ_R, i.e., $\sigma_R(^{40}Ar)/\sigma_R(H) = 3.5\ A^{1/3}(proj)$.

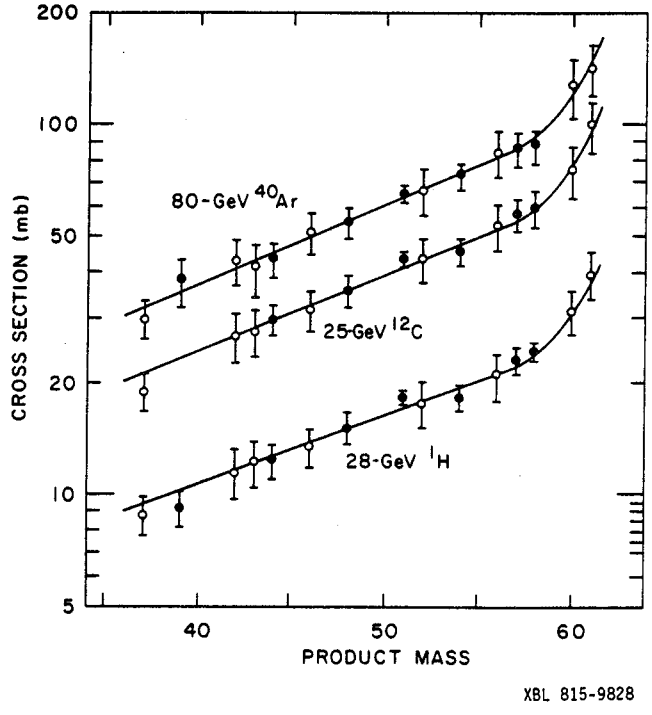

Fig. 1. Mass-yield curves from the fragmentation of Cu. Vertical scale for ^{12}C is arbitrary.

Figure 2 gives the energy dependence of the slopes of the exponential mass yield curves in the region $37 \lesssim A_f \lesssim 57$ for the fragmentation of Cu by protons, $0.35 \leq T_p \leq 28$ GeV, ^{4}He at 0.41 and 0.72 GeV, 3.9-GeV ^{14}Ne, 25-GeV ^{12}C and 80-GeV ^{40}Ar. A key result here is that the data are ordered when plotted as a function of total kinetic energy of the projectile nucleus, rather than velocity or rapidity, i.e., kinetic energy per nucleon. Furthermore, the onset of limiting fragmentation is evident for total kinetic energies $T \gtrsim 2$ GeV, with notable similarity between protons and heavy ions in terms of their energy deposition. Evidence supporting these conclusions has come from experiments on

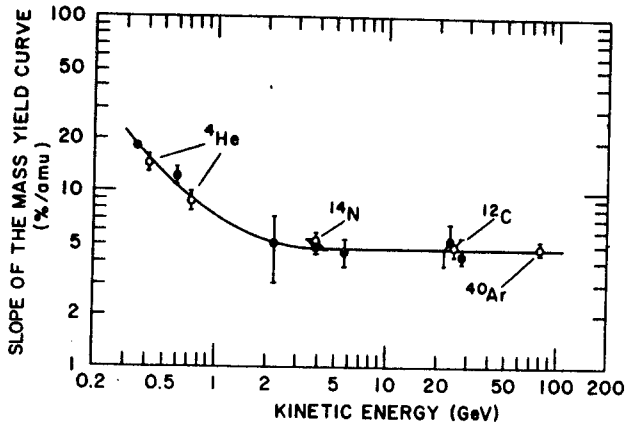

XBL 815-9829

Fig. 2. Slope of mass-yield curves from the fragmentation of Cu as a function of kinetic energy of the beam projectile. Filled circles are for protons.

the fragmentation of Ag by 25-GeV ^{12}C and 300-GeV protons (ref. 12), ^{181}Ta by 8.0-GeV ^{20}Ne (ref. 13,14), and ^{197}Au by 4.8- and 25-GeV ^{12}C (ref. 15) and 8.0 (7.6)-GeV ^{20}Ne (ref. 13,15), and ^{238}U by 4.8-GeV ^{12}C and 5.0-GeV ^{20}Ne (ref. 16).

The radiochemical technique is also applicable to studies of the recoil properties of isotopically identifiable target residues. Such studies have been found to be particularly sensitive tests of limiting fragmentation as it applies to the asymptotic kinematic limits of the target recoil velocities. Measured in these experiments are the fractions of each nuclide that recoil out of a thin target in the forward and backward directions. By assuming that the recoil fragments result from a two-step (fast-slow) process, the observations can be interpreted in terms of the mean forward-directed velocity $\langle\beta_\parallel\rangle$ of the prefragment produced in the primary projectile-target interaction and the mean Maxwellian-distributed velocity $\langle\beta\rangle$ that arises from the de-excitation of the prefragment to produce the observed residue. The model assumes that $\vec{v} = \vec{\beta}c$ is isotropically distributed in the moving frame ($\beta_\parallel$) of the prefragment.

The principal characteristics of the velocities $\langle\beta_\parallel\rangle$ and $\langle p\rangle$ deduced from experiment via the two-step model[17] are illustrated in Figs. 3 and 4. Figure 3 summarizes the dependence of the mean longitudinal recoil velocity of the first step, $\langle\beta_\parallel\rangle$, on the mass number of the detected fragment. These data were collected from the works of Loveland[14] and Kaufman and co-workers[15,18] and include both proton and heavy ion beams in the (kinetic) energy range 3-28 GeV, incident on ^{197}Au and ^{181}Ta. The qualitative features of the recoil velocities $\langle\beta_\parallel\rangle$ are: i) their small values, typically $\lesssim$1% of the beam velocities, and ii) their inverse dependences on fragment mass A_F, especially in the range $24 \leqslant A_F \leqslant 100$, and beam energy, where $\langle\beta_\parallel\rangle$ is observed to decrease with increasing beam energy, the $\langle\beta_\parallel\rangle$ vs. A_F relationship becoming indistinguishable for protons at 28 GeV and ^{12}C at 25 GeV. These results illustrate well that $\langle\beta_\parallel\rangle$ approaches a limiting value in the spirit of limiting fragmentation and that beam independence is essentially attained at total kinetic energies $T \gtrsim 25$ GeV.

The most interesting feature of Fig. 3 to me is that the recoil velocities $\langle\beta_\parallel\rangle$ are inversely proportional to the mass of the fragment, A_F, particularly for $A_F \leqslant 100$. This leads to the suggestion that the loci of data points can be expressed rather well in terms of a characteristic mean momentum $P_0 = 931\ A_F\ \langle\beta_\parallel\rangle$ MeV associated with each plot of $\langle\beta_\parallel\rangle$ vs. A_F. For the data shown, I have evaluated P_0 from the unweighted data for $\langle\beta_\parallel\rangle$, with $A_F \leqslant 100$, and have

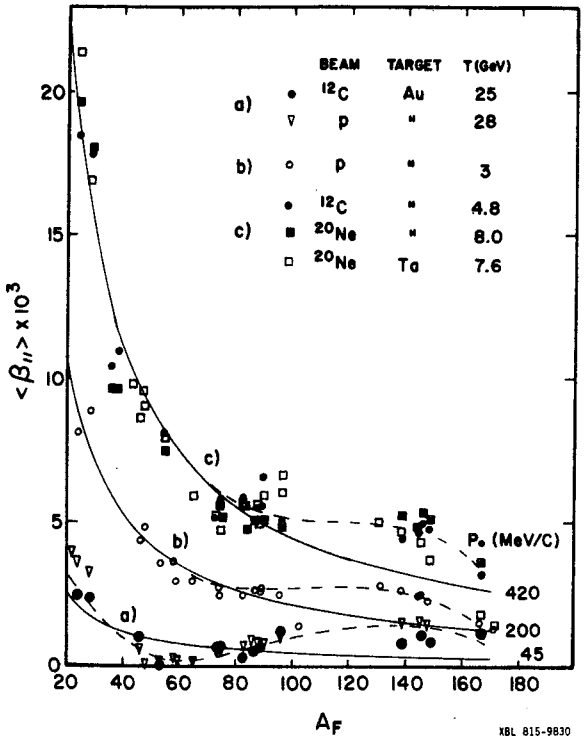

Fig. 3. Longitudinal recoil velocity of fragment of mass number A_F as a function of beam and beam energy. Solid curves are $<\beta_{\parallel}> = P_0/931\ A_F$ for the values of P_0 indicated. Dashed lines delineate data points.

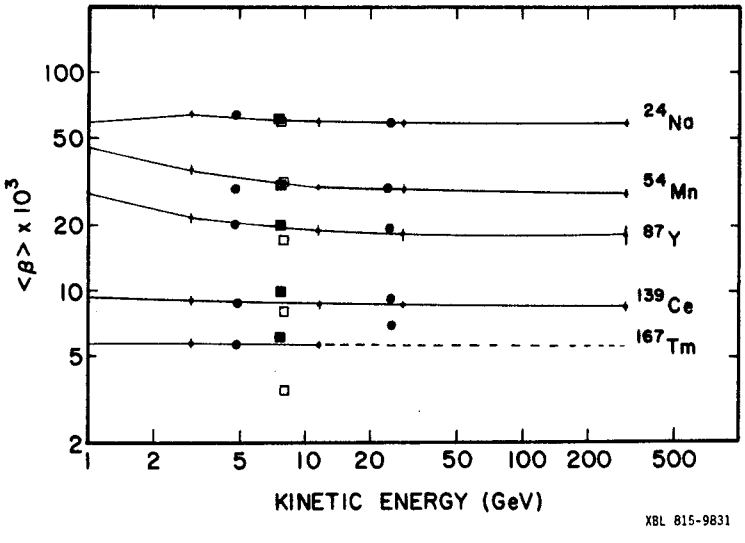

Fig. 4. Mean velocity of fragments indicated from de-excitation stage as a function of mass and energy of projectile. Symbols are: for Au target, ♦, protons (ref. 18); ●, ^{12}C (ref. 15); ■, ^{20}Ne (ref. 15); and for Ta target, □, ^{20}Ne (ref. 14).

drawn the resultant curves of the expression $\langle\beta_{\parallel}\rangle = P_o/931\ A_F$, where the values of P_o corresponding to curves a), b), and c) in Fig. 3 are 420 ± 7 MeV/c, 200 ± 6 MeV/c, and 45 ± 6 MeV/c, respectively. Although admittedly an oversimplification, the data are compatible with $A_F\langle\beta_{\parallel}\rangle$ = constant over most of the range of fragment mass, with the largest deviations occurring at high beam energies (curve c) and, in all cases, for $A_F \approx 140$.

Figure 4 illustrates that the mean velocity $\langle\beta\rangle$ of a given fragment that arises from the de-excitation stage is, to good approximation, independent of the mass and kinetic energy of the projectile to beam energies $T \geq 3$ GeV. These data support the basic assumption that the de-excitation stage is independent of the kinematics of its formation, consistent with a relatively long time scale compared to that of the initial interaction.

Having demonstrated that the quantities $\langle\beta_{\parallel}\rangle$ and $\langle\beta\rangle$ exhibit the properties appropriate for a two-step process, let us delve into the (approximate) kinematics of the two-step model. By doing so, one obtains a kinematic interpretation of the quasi-invariance of $P_o \propto A_F\langle\beta_{\parallel}\rangle$ and a means for describing the asymptotic approach of $\langle\beta_{\parallel}\rangle$ to a limiting value at high beam energies.

The two-step kinematic model I adopt is that proposed by Masuda and Uchiyama[19], which describes target fragmentation by the sequence of reactions, i) $B + T \rightarrow B^* + T^*$ and ii) $T^* \rightarrow F + X$, whereby the target (projectile) nucleus T(B) is excited to the state T*(B*), the decay of which leads to the detected target (projectile) fragment F. This model has been used successfully in the interpretation of projectile fragmentation data at relativistic[19] as well as nonrelativistic energies[20].

Given the approximations that the recoil << excitation << nuclear rest energies and that the excitation energies of the target and beam nuclei are, on the average, equal (considering pionic degrees of freedom, this approximation is applicable to proton beams), the conservation of energy and momentum leads to the following expression for the recoil velocity $\langle\beta_{\parallel}\rangle$ of the target system:†

$$\langle\beta_{\parallel}\rangle = \frac{E^*}{M_T}\sqrt{\frac{\gamma+1}{\gamma-1}} \quad , \tag{1}$$

where E* is the excitation energy of the target (projectile), M_T is the mass of the target, and γ is the Lorentz factor of the beam nucleus. Given the approximate constancy of the mean momentum $P_o = M_F\langle\beta_{\parallel}\rangle$ of the fragments at beam energy $M_B(\gamma-1)$ as depicted in Fig. 3, the following relation holds:

$$M_F E^* = P_o M_T \sqrt{\frac{\gamma-1}{\gamma+1}}, \text{ with } Po = f(\gamma-1) \quad . \tag{2}$$

Simple kinematics of the two-step model, incorporating the observation $P_o = M_F\langle\beta_{\parallel}\rangle$, thus indicates that the quantity $M_F E^*$ is a constant for a given beam energy and that E* is linearly related to the mean recoil velocity $\langle\beta_{\parallel}\rangle$ of the fragment F, Eq. 1. This latter feature has been previously demonstrated in a variety of intranuclear cascade calculations.[18,21]

In Fig. 5, I have plotted $M_F E^*$ (Eq. 2) versus beam kinetic energy for a variety of beam and target nuclei, using the values of P_o extracted from published $\langle\beta_{\parallel}\rangle$ vs. A_F data.[14,15,16,18] Again, the data are ordered by the kinetic energy of the beam and show that E* associated with each fragment mass attains a maximum near 5 GeV, decreasing thereafter with increasing beam energy, approaching an asymptotic value for energies $\gtrsim$ 25 GeV. Within experimental

---

†Derived from relativistic energy conservation with the approximation that neglects all quadratic terms of the recoil momentum and excitation energies. The nonrelativistic expression for the recoil momentum is also used.

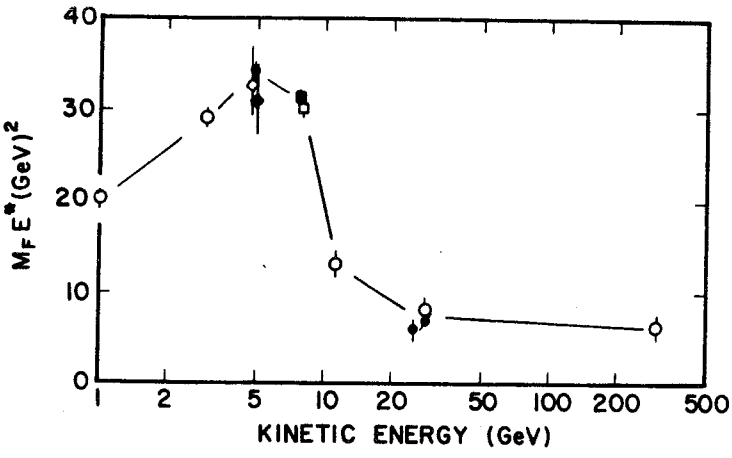

Fig. 5. The product of fragment mass and excitation energy as a function of beam energy and mass. Symbols are: for Au target, ○ protons, ● ^{12}C, ■ ^{20}Ne; for Ta target, □ ^{20}Ne, and for U target, ◇ ^{12}C and ◆ ^{20}Ne. Data are compiled from Refs. 14, 15, 16 and 18.

errors E*(25 GeV) ≡ E* (300 GeV). Limiting fragmentation is thus satisfied for the variable $M_F E^*$ for beam energies >25 GeV. Because $\langle\beta_\parallel\rangle \propto E^*$, Eq. 1, the recoil velocity $\langle\beta_\parallel\rangle$, which is the kinematic quantity that controls the forward/backward ratio of fragments, also attains a limiting value at beam energies $\gtrsim$ 25 GeV. Other obvious conclusions from Fig. 5 are: i) the fragment angular distributions in the laboratory, because of their dependence on $\langle\beta_\parallel\rangle$, will exhibit maximum asymmetries in the laboratory at beam energies ~5 GeV, ii) limiting fragmentation is clearly not met for energies $\lesssim$10 GeV, iii) the scaling factor that "universally" interrelates $\langle\beta_\parallel\rangle$ and E* for beam nuclei $1 \leq A_B \leq 20$ for which data are available is the total kinetic energy of the beam, and iv) the excitation energies, hence $\langle\beta_\parallel\rangle$, are independent of the projectile mass, i.e., factorization is valid, as indicated by Eq. 1.

The important conclusion to come from these target fragmentation experiments is that it is the total kinetic energy of the projectile, rather than its velocity, that is relevant to the physics of these RHI interactions. Similar conclusions have also been made from the experiment of Sandoval, et al.[22], where it was found that the associated multiplicities varied smoothly with, and depended only on, the total kinetic energy of the projectile. By associated multiplicity we mean the multiplicity of particles that is associated with the coincident detection of a given fragment in a single-particle inclusive experiment. The multiplicity array used by Sandoval, et al. was sensitive to particles having kinetic energies $\gtrsim$25 A MeV.

Figure 6 gives the average associated multiplicities <M> emitted from a U target (associated with a coincident proton 40 < T < 200 MeV detected at 90° to the beam) plotted as a function of the energy and mass of the projectile. It is clear that <M> depends on the total kinetic energy of the beam, with the equivalent behavior for protons and heavy nuclei again demonstrated. Furthermore, not only averages, but the (observed) associated multiplicity distributions, are virtually identically at the same beam kinetic energies. This is shown in Fig. 7 for ^{40}Ar and ^{20}Ne projectiles at 42 GeV.

That the total kinetic energy of the projectile orders both the mass-yield curves from the radiochemical experiments and the associated multiplicity data indicates that the physics beneath these rather diverse observations are

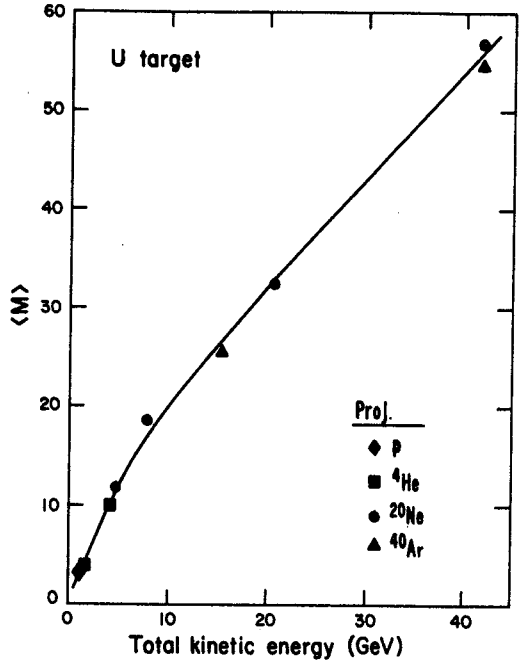

XBL 797-2054

Fig. 6. Average associated multiplicities as a function of total kinetic energy for various beam nuclei on uranium.

related, as indeed they are. Because the associated multiplicities measured predominantly light, energetic fragments from the target, they are the complements of the residues of the target nuclei, hence related to the mass yield curves.

I would like to point out the observation that even for the lowest values of the multiplicities m, Fig. 7 (where one normally would assume the collisions to be heavily biased towards peripheral collisions, hence towards large impact parameters), no discernible difference between the m-distributions for ^{40}Ar and ^{20}Ne projectiles is evident. It is just from this type of collision that one generally attributes to the production of the large target residues, i.e., the target "spectators", that are subject to radiochemical analyses.

A conclusion one is almost forced to, then, is that the target "spectators" sense, in some coherent way, the energy of the entire incident beam nucleus, rather than the kinetic energy of the individual nucleons, irrespective of the projectile mass and impact parameter. We are seeing an effect that is truly nuclear. An explanation of these, as well as some very recent results on the "explosive" reactions of 1.7 A GeV ^{56}Fe observed in nuclear emulsions[23], must invoke $p_\perp$-effects that effectively increase the "transverse communication" between the geometrically defined spectator and participant nucleons.

3. Pion Interferometry: Source Sizes

Independently proposed by Cocconi[24] and Kopylov, Podgoretsky and co-workers[25,26] was that the principle of intensity interferometry can be applied to systems of hadronic dimensions. This is a well-known astronomical

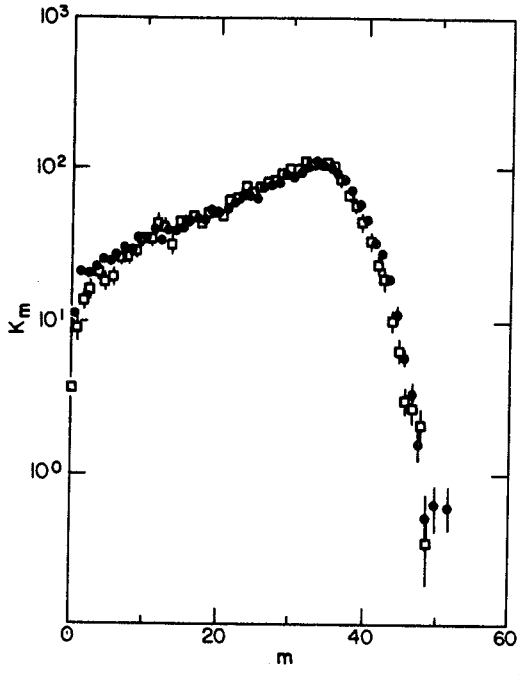

XBL 797-2052

Fig. 7. Coincidence probability distributions for 42 GeV ^{20}Ne and ^{40}Ar incident on uranium. Symbols are □, ^{20}Ne and •, ^{40}Ar.

technique developed and first used by Hanbury-Brown and Twiss to measure the apparent angular diameter of Sirius.[27] In analogy to the Hanbury-Brown and Twiss effect, the correlations between simultaneously emitted identical bosons, i.e., pions, can be used to establish the space-time dimensions of the interaction region from which they are emitted.

The principle of pion interferometry is schematically illustrated in Fig. 8, which depicts an event in which a pion, π_1, with four-momentum p_1 is detected at space-time x_1, in coincidence with a second pion, π_2 with p_2 at x_2. Owing to the space-time extension of the source, the coincident event can occur in two ways; either π_1 is emitted from r_1 and π_2 from r_2 (solid lines) or the π_2 is emitted fron r_1 and π_1 from r_2 (dashed lines). Because the two possible configurations are indistinguishable in producing a coincidence, the total amplitude ψ of the event is, for pions, the sum of the partial amplitudes. The coincidence rate, assuming plane waves, is proportional to the probability

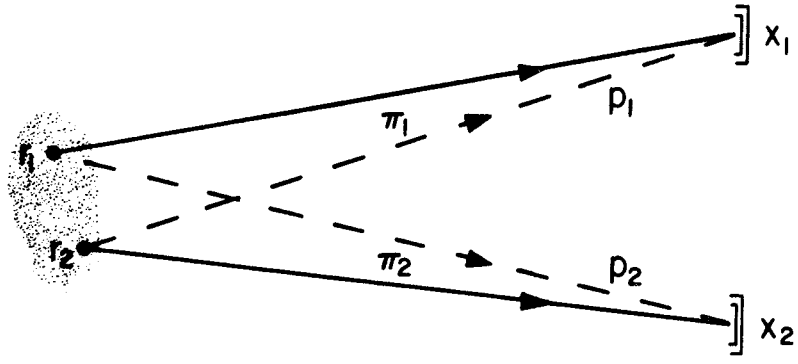

XBL 815-9836

Fig. 8. Possible configurations of a two-pion coincidence event.

$$|\psi|^2 \propto |\exp\{i[p_1\cdot(x_1 - r_1) + p_2\cdot(x_2 - r_2)]\}$$
$$+ \exp\{i[p_1\cdot(x_1 - r_2) + p_2\cdot(x_2 - r_1)]\}|^2$$
$$\propto 1 + \cos[(p_1 - p_2)\cdot(r_1 - r_2)] \quad . \tag{3}$$

With $p = (E,\vec{p})$ and $r = (t,\vec{r})$, we have

$$|\psi|^2 \propto 1 + \cos[q_0(t_1 - t_2) - q\cdot(\vec{r}_1 - \vec{r}_2)] \quad , \tag{4}$$

where $q_0 = E_1 - E_2$ and $\vec{q} = \vec{p}_1 - \vec{p}_2$ in the CM system.

The coincidence rate measured as functions of q_0 and q for pairs of like pions will therefore exhibit a modulation, i.e., a second-order interference effect, from which the characteristic space-time dimensions of the pion-emitting source can be determined. Because r_1 and r_2 represent but two distinct emitters in the source, the observed coincidence rate R is obtained by integrating $|\psi|^2$ over the space-time distribution $\rho(r)$ of the source. An analytic expression for R that is most commonly used to extract the characteristic space-time parameters of the source from the experimental data is based on an assumed Gaussian distribution of the form $\rho(t,r) \sim \exp-[r^2/r_0^2 + t^2/\tau^2]$, which results in a coincidence rate given by

$$R(q,q_0) \sim 1 + \exp\left(-\frac{\tau^2 q_0^2}{2} - \frac{r_0^2 q^2}{2}\right) \quad , \tag{5}$$

where r_0 and τ are the space-time parameters of the source.[28] The saliant features of $R(q,q_0)$ are: i) for pions of the same charge there is <u>constructive</u> interference, an effect of the Bose-Einstein statistics, as $\vec{q} \to 0$,

i.e., the pions have the same momentum vectors, and as $q_0 \to 0$, i.e., the pions have equal energy and ii) $R(q,q_0)$ decreases from a maximum value of 2 at the origin monotonically approaching a plateau value of 1 for $q_0 \gg \tau^{-1}$ and for $|q| \gg r_0^{-1}$.

The most crucial aspect of an experimental measurement of the two-particle correlation function is the determination of the background distribution in the absence of Bose-Einstein correlations. The procedure that has been adopted in RHI experiments is that suggested by Kopylov[25], which is to construct an uncorrelated background distribution by selecting each like-pion from a different event. Although the procedure clearly establishes the pions to be uncorrelated, it is not without inherent difficulties. For example, momentum is not conserved (this should, however, introduce minimal effects because of the large number of final-state particles in RHI interactions), and, second, the procedures and methods to evaluate the statistical significance of the background spectra so generated are obscure and not fully established. Consequently, the systematic errors introduced into the resultant source parameters r_0 and τ deduced from experiments have yet to be assessed.

The first application of pion interferometry to RHI collisions was by Fung, et al.[29] who carried out a study of $2\pi^-$ correlations in reactions of 1.8-A GeV ^{40}Ar beams with heavy target nuclei positioned in the LBL streamer chamber. Representative data from this experiment are given in Fig. 9, which

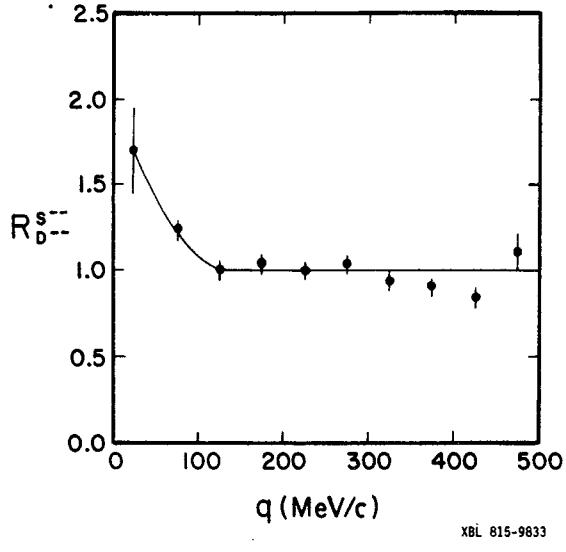

Fig. 9. Kopylov ratio R_{D--}^{S--} versus relative pion momentum q. 1.8-A GeV ^{40}Ar beam incident on Pb_3O_4, "central" trigger.

gives the ratio R_{D--}^{S--}, i.e., the normalized ratio of the number of π^- pairs from the same event to the number of π^- pairs from different events (bin by bin), versus q(MeV/c) for events from a Pb_3O_4 target selected by a "central collision" trigger mode. The data show a clear enhancement of low values of q. The parameters extracted from these data are listed in Table 1. A re-analysis of these data has subsequently been made by subgrouping the events into different pion multiplicities.[30] As tabulated in Table 1, the pion source is seen to increase from 3.1 ± 1.1 to 5.6 ± 1.2 fm as the pion multiplicity increases from the interval 2-4 to 13-15. Because of the insensitivity of the

Table 1
Pion interferometry analysis based on Gaussian source-density distribution, Eq. 5. $c\tau$ is either estimated or set to 1.5 fm. Gamov-corrected values of r_o are indicated by *. Beam is ^{40}Ar at 1.8 A GeV in all cases.

Pair	Target	N_{π^-}	r_o(fm)	$c\tau$(fm)	Ref.
$2\pi^-$	Pb_3O_4	2-15	3.98 ± 0.78	$0.6 \begin{smallmatrix}+1.2\\-0.5\end{smallmatrix}$	29
$2\pi^-$	"	2-4	3.12 ± 1.10	$\equiv 1.5$	30
$2\pi^-$	"	5-8	4.00 ± 0.72	1.5	30
$2\pi^-$	"	9-12	4.82 ± 0.65	1.5	30
$2\pi^-$	"	13-15	5.57 ± 1.71	1.5	30
$2\pi^-$	KCl		$1.84 \begin{smallmatrix}+0.27\\-0.25\end{smallmatrix}$	1.5	35
$2\pi^-$	"		2.98 ± 0.30*	1.5	35
$2\pi^+$	"		$1.60 \begin{smallmatrix}+0.55\\-0.40\end{smallmatrix}$	1.5	35
$2\pi^+$	"		3.85 ± 0.45*	1.5	35

value of r_o to the lifetime parameter, $c\tau$ is set to 1.5 fm for this analysis. The principal features of the r_o parameter that characterizes the $2\pi^-$ correlation data from this streamer chamber experiment are:

i) r_o is comparable to the radius of the ^{40}Ar projectile nucleus $\sim 1.2\ A^{1/3} = 4.1$ fm, incompatible with the (fermi momentum) values of $r_o \approx 1$ fm $\approx \hbar/p_f$ obtained from 2π correlations in pp (ref. 31) and πp (ref. 32) collisions.

ii) r_o increases monotonically with the pion multiplicity, indicative of a correlation between the size of the pion source with the degree of excitation energy in the collision.

iii) the pion multiplicity N_{π^-} appears to be proportional to r_o^3, the volume of the pion-emitting source.

iv) When compared to the thermodynamic model of Gyulassy and Kauffmann,[33] the values of r_o are more consistent with a nuclear freeze-out density $\rho_c \approx \rho_o$ (normal nuclear density) than with the typically assumed value of $\rho_c \approx \rho_o/3$.[34]

The analysis by Lu, et al.[30] follows directly from Eq. 5 and does not take into account corrections for the relative Coulomb interactions between the pions (in their CM), Coulomb effects owing to the nuclear charges, and possible final-state interactions. That such corrections may be significant comes from the analysis by Bistirlich, et al.[35] of their experiment on $\pi\pi$ correlations in the reaction $^{40}Ar + KCl \rightarrow 2\pi + X$ at 1.8 A GeV. In this experiment a magnetic spectrometer was used to measure the momenta of the like-pions (either ++ or --) in the range $200 \leq p \leq 800$ MeV/c, emitted within a solid angle $\sim$0.1 msr at lab angles 40 to 50°. Bistirlich, et al. have shown that the most significant, and most tractable, correction is that due to the 2π relative Coulomb interaction. At low relative momentum, q_{rel}, in the 2-pion system, Coulomb repulsion between the pions suppresses the number of events in the observed ratio $R(q,q_0)$ at low values of q. The correction for this effect is given by the expression $n_{corr} = G(\eta)^{-1} n_{obs}(q)$, where n(q) denotes the density of events at q and $G(\eta)$ is the Gamov function

$$G(\eta) = 2\pi\eta/(e^{2\pi\eta} - 1), \text{ with } \eta = m_\pi c/137 q_{rel} \quad . \tag{6}$$

To stress the importance of this effect, at $q_{rel} = 5$ MeV/c, $G(\eta) = 0.5$--which is sufficient to suppress completely any Bose-Einstein enhancement that might be present.

The effect of the Gamov correction on the correlation function is demonstrated in Fig. 10 and therefore on the estimates of r_0 in Table 1. The corrected estimates of r_0 (with $c\tau \equiv 1.5$ fm) obtained by Bistirlich, et al. are typically 1-2 fm larger than the uncorrected values of r_0. This is shown

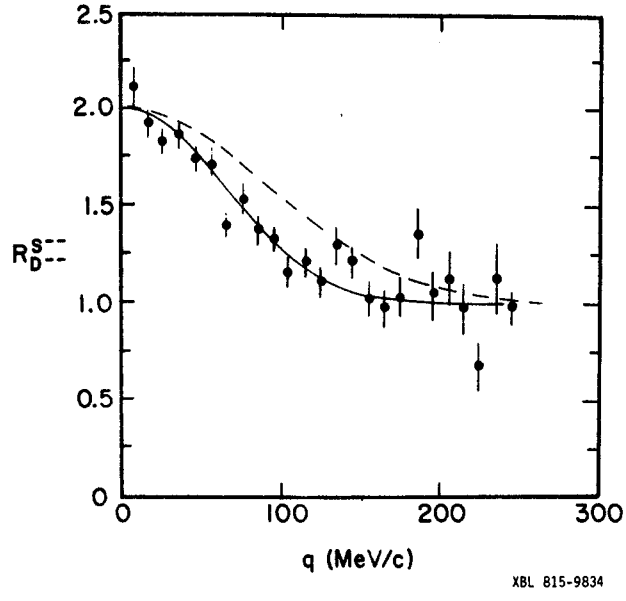

Fig. 10. Kopylov ratio versus relative pion momentum; 1.8 A GeV ^{40}Ar incident on KCl. Gamov-corrected data with fitted (solid) curve are shown. Dashed curve is fit to uncorrected data.

in Fig. 10, where the Gamov-corrected $2\pi^-$ correlation data are plotted. The solid line corresponds to a (Gaussian) source of $r_o = 2.98 \pm 0.30$ fm and $c\tau \equiv 1.5$ fm. The dashed line indicates the fit to the data before the Gamov correction is made, the (uncorrected) parameters in this case being $r_o = 1.84 \pm 0.27$ fm and $c\tau \equiv 1.5$ fm.

Demonstrated by these initial RHI experiments on pion interferometry is that the space-time structures, and even coherence, of the pion-emission sources are subject to experimental study. They also have pointed out technical and sensitive analytical problems that must be fully understood and resolved if we are to probe the actual size and shape of the pion source. That the space/time properties of the interaction volumes appear to be correlated with the associated pion multiplicities clearly adds new dimensions to the problem and certainly enhances our ability to get to the "heart of the matter".

4. The Short MFP Phenomenon: Anomalons?

In 1954, six years after the discovery of the heavy ion component in cosmic rays, the first disquieting evidence emerged for projectile fragments (PF) from RHI collisions having, apparently, anomalously short reaction mean free paths (MFP). (See ref. 36 and references therein.) Although subsequent cosmic ray experiments through 1972 extended and generally supported such evidence, it was not until beams of accelerated nuclei became available that the technical and statistical limitations of the cosmic-ray experiments could effectively be eliminated and the problem systematically pursued. Two Bevalac experiments that have focused on the interaction properties of relativistic PFs in nuclear research emulsions have been carried out, the first by B. Judek, NRC, who studied the PFs of ^{16}O at 2.1 A GeV and the second at LBL, where ^{56}Fe projectiles at 1.9 A GeV were used. The scanning and measuring of these experiments were done independently at the respective laboratories; the analysis of the data from each experiment was carried out at LBL. The results of the NRC and LBL experiments were compatible with each other, hence have been combined to improve the statistical accuracy of the final result.[36]

The emulsion stacks used in the experiments were fabricated with Ilford G.5, 600-μm-thick pellicles, with stack I (NRC) containing 50 pellicles, 15 x 30 cm^2 and stack II (LBL) 41 pellicles, 7.5 x 12 cm^2. The stacks were exposed with the beams normal to their entry faces, parallel to the surface planes of the pellicles. Scanning of the pellicles was performed by picking up the entering beam nuclei within a few mm from the entrance edge and following along each individual beam track until it either interacted or left the stack (NRC) or pellicle (LBL). An interaction is defined to be one that involves the emission of at least one observable hadronic track, from either the projectile or target nucleus. Interactions involving i) neutron emission only and ii) low-momentum transfer elastic nucleus-nucleus scattering are therefore excluded from the data. All relativistic tracks $Z \geq 3$ emitted from the primary, secondary, tertiary... interactions within a 100-mrad forward cone were followed until the topology of each event was completely determined. Charge measurements to $|\Delta Z| \gtrsim 1$ unit were carried out for all fragments, under the assumption that projectile fragments are produced at beam velocity.

Figure 11 is a microprojection drawing of a characteristic type of event observed in the experiments: a linear chain of successive PF interactions. In this event, a (first generation) ^{56}Fe projectile initiates a succession of projectile fragmentations that gives rise to leading fragments of charge Z = 24, 20, and 11 in the second through fourth generations, respectively. Because no PF with $Z \geq 3$ is emitted from the fourth generation, the event terminates at this point. The largest chain of this type was observed at NRC where the sequence was $^{16}O \rightarrow N \rightarrow C \rightarrow B \rightarrow B \rightarrow B \rightarrow Be \rightarrow He$ (out stack), a 7-generation event. Note that the interactions in Fig. 11 are characteristic of high-energy, hardonic interactions, namely, the projectile fragments are confined to a narrow

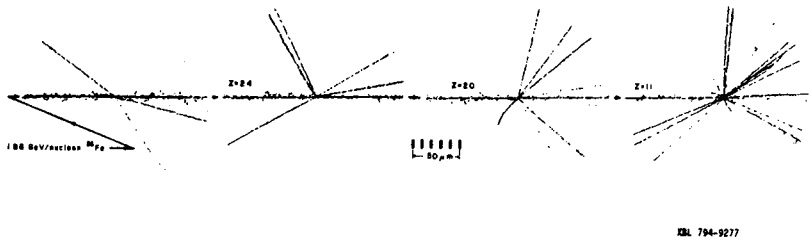

XBL 794-9277

Fig. 11. A succession of (4) fragmentation reactions initiated by a 1.9 A GeV ^{56}Fe (enters from the left). Actual distance between first and final interactions is 5.7 cm.

forward cone, with significant particle production and target excitation being evident.

The data base consists of a total of 1456 interactions, second through seventh generations inclusive. The following quantities were measured for each PF: i) charge Z, ii) potential path T available for interaction in the emulsion detector, and, if it interacted, iii) the distance X to its interaction point. From these data, the MFP for PFs of charge Z, λ_Z^*, is given by

$$\lambda_Z^* = \Sigma S_i / N_Z \quad , \tag{7}$$

where ΣS_i is the total path length followed for both interacting and noninteracting tracks that leads to N_Z interactions. The estimate of the MFP by this procedure is independent of the stack size and/or potential path T. This is illustrated in Fig. 12, where the value of λ^* observed for primary ^{16}O beam nuclei for each 1 cm interval is plotted as a funtion of distance D from the scan-line (pick-up point) of incident nuclei. In effect, the 30 cm long emulsion detector is segmented into 30 independent, 1 cm long, detectors. The data are well accounted for by a constant value of λ^* as expected by Eq. 7, the straight-line fit to the data at $\overline{\lambda^*}$ = 11.9 cm having a χ^2 = 20, 29 DOF.

The ^{16}O data are representative of a series of MFP measurements of beam nuclei, varying from ^4He to ^{56}Fe, which, by definition, are taken to be the "normal" MFPs of nuclei. A useful result of the MFP measurements of beam nuclei is that they can be parameterized as

$$\lambda_Z = \Lambda Z^{-b} \quad , \tag{8}$$

where the Λ for beam nuclei is Λ_{beam} = 30.4 ± 1.6 cm and b = 0.44 ± 0.02. This expression approximates well calculations of MFPs in emulsion based on geometrical-overlap models. It also enables one to reduce all measurements of λ_Z^* (Eq. 7) of the PFs to a single parameter, Λ^*, given by the expression

$$\Lambda^* = \Sigma_Z \lambda_Z^* N_Z Z^b / \Sigma_Z N_Z \quad . \tag{9}$$

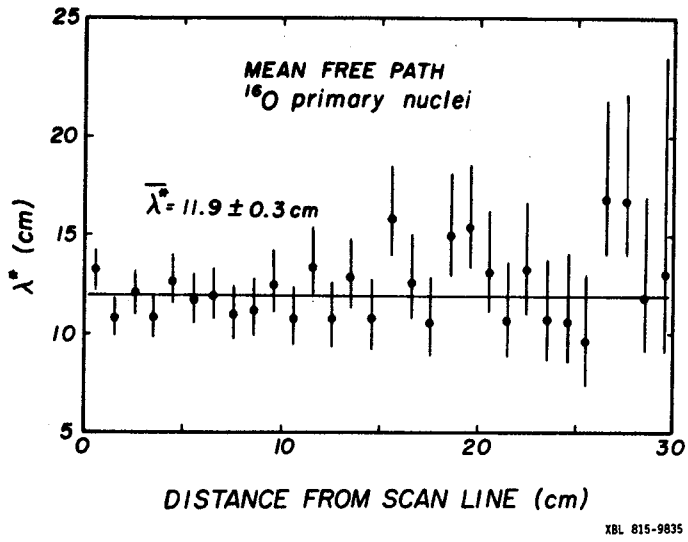

Fig. 12. Measured values of MFP of incident 2.1 A GeV ^{16}O as a function of distance from scan line, stack I (NRC).

Figure 13 presents the mean-free-path parameter Λ^* for PFs (all generations combined), plotted as a function of distance D from the origin of emission of the PF. In contrast to the ^{16}O beam data, Fig. 12, the values for Λ^* are low for the first several centimeters, becoming compatible with Λ_{beam} for D $\gtrsim$ 5 cm. The difference between the observed MFPs of PFs and their

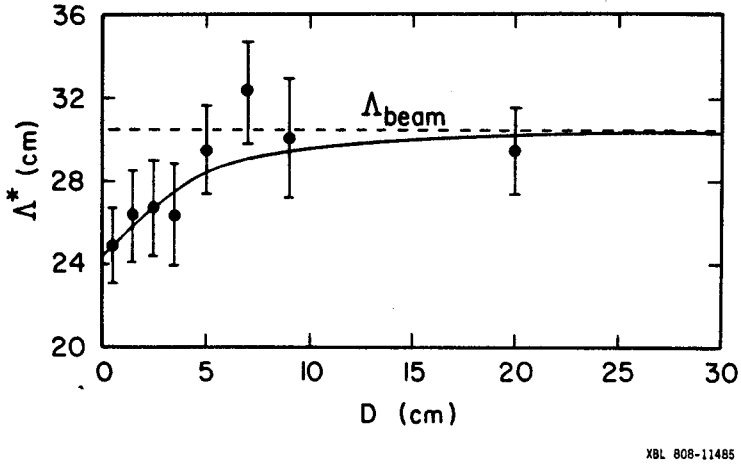

Fig. 13. MFP parameter Λ^* versus distance from origins at PFs: full circle, experiment; dashed line, prediction from Λ_{beam}; solid line, prediction assuming 6% admixture of PFs with λ_a = 2.5 cm.

expected values based on beam calibrations exceed 4.5 standard deviations. The short MFPs at small distances D mean that there is an excess in the number of interactions at these distances. To obtain some insight as to the nature of this excess of interactions of PFs at short distances, a most elementary assumption can be made: In addition to normal nuclei, there is a component of "anomalons", PFs that are produced with probability $\underline{a}$, having a constant, "anomalously short" MFP, λ_a. Estimates of $\underline{a}$ and λ_a from the data give $\underline{a}^* \approx$ 6% and $\lambda_a^* \approx 2.5$ cm. (For comparison: $\lambda(^{56}Fe) \approx 7.3$ cm, $\lambda(^4He) \approx 22$ cm.)

The solid curve through the data, Fig. 13, is the computed D vs Λ^* based on these parameters. Although this primitive model is compatible with the experimental data, it is quite clear that it is not necessarily a unique one.

A criticism of the above analysis is that it depends on the comparison of the MFPs of PFs with the predictions obtained from the approximate parametric expression for the MFP of beam nuclei, Eq. 8. An analysis of the data that is independent of this parameterization is to test whether two estimates of λ. say λ_1^* and λ_2^*, are compatible with the assumption that they are sampled from the same distribution. This is done by computing the ratio $F = \lambda_2^*/\lambda_1^*$, which propitiously obeys the well-known F-variance ratio distribution. Given the number of events N_2 and N_1 used to evaluate λ_2^* and λ_1^*, the probability P(<F), which is the integral of the F-variance ratio distribution, can be evaluated for the ratio F. The important feature of P(<F) is that it is uniformly distributed between 0 and 1, with <P> = 0.5 provided λ_2^* and λ_1^* are, in fact, from the same distribution.

This test was made for two cases, where λ_2^* and λ_1^* are i) the values of λ_Z^* of the PFs for distances D $\leq$ 2.5 and > 2.5 cm and ii) the values of λ_Z^* for the third (and higher) and second generation PFs. The results are shown in Fig. 14, which gives in histogram form the values of P(<F) for each pair of λ^* values. The shaded areas identify the (6) ratios from the NRC data to show the agreement between the laboratories. The distributions of P(<F) do not appear to represent

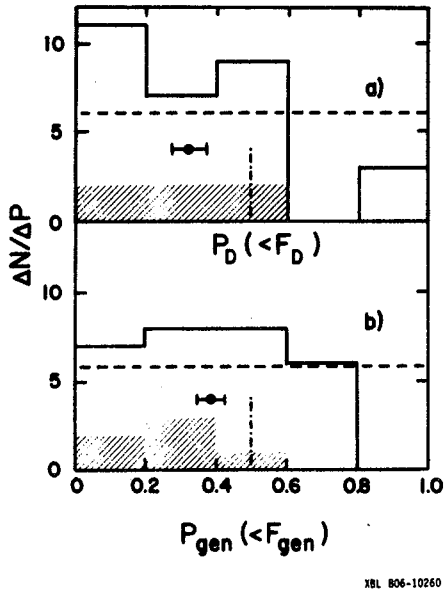

Fig. 14. Frequency distributions a) $P_D(F_D)$ for λ_Z^* ($\leq$D) and λ_Z^* (>D), with D = 2.5 cm, b) P_{gen} ($<F_{gen}$) for λ_Z^* (3rd and higher gen) and λ_Z^*(2nd gen). Mean values indicated are to be compared with expectation value <P> = 1/2.

uniform distributions (indicated by the dashed lines) in either case. The means <P> of the observed distributions are -3.4 SD (Fig. 14a) and -2.1 SD (Fig 14b) from the expectation values of 1/2. The conclusions drawn from these distributions are: from Fig. 14a, the MFPs of PFs at short distances D from their points of emission are significantly shorter than the MFPs at longer distances, independent of any hypothesis as to the dependence of the MFP and Z, methods and efficiency of scanning and other possible inter-lab differences; and from Fig. 14b, the MFP of tertiary and higher generations of PFs appear to be shorter, as a whole, than the MFP of secondary PFs. Although the statistical significance of this generation effect is not particularly strong (2.1 SD), the result does suggest the presence of a "memory" phenomenon, which infers that once an "anomalon" is produced, it tends to persist in subsequent interactions.

Taken at face value, the LBL-NRC experiment have sustained the early cosmic-ray evidence for a short MFP component among the PFs of RHI. Barring the possibility that the results are attributable to a statistical fluctuation of probability $\lesssim 5 \times 10^{-4}$, the observations are compatible with a (presumably) multibaryon state that interacts with matter with cross sections 3-10 times larger than those of beam nuclei of the same charge. To affect a $\lambda \approx 2.5$ cm, such a multibaryon state would have to have an effective interaction radius about 3 fm larger than that of a uranium nucleus.

Such a conclusion, obviously, is a profound one, and other possible interpretations of the experiment must be explored. Systematic errors arising from scanning techniques, gross arithmetic mistakes, errors in charge assignments, and the assumption of the persistence of (beam) velocity of the PFs have been examined by rescanning, Monte Carlo calculations, etc. and have been shown unable to explain the observations. Conventional explanations invoking excited states of conventional nuclei, hyperfragment decay, background stars owing to neutrons, and the superposition of particle tracks either do not lead to MFPs as short as $\sim$2.5 cm or can be directly rejected by comparing the topologies of the interactions of PFs and beam nuclei.

A new experiment by the LBL-NRC-Marburg collaboration is now underway to extend and amplify the foregoing results. Measurements on Z = 2 PFs from ^{56}Fe interactions in emulsion at 1.9 A GeV are in progress, as are a series of calibration measurements for MFP and charge for 2 A GeV beams of ^{3,4}He, ^{6}Li, ^{12}C and ^{40}Ar. The advantage of a Z = 2 PF experiment are: i) low rate of Z misidentifications, ii) no excited states in the He system, iii) the PFs are predominantly ^{3}He and ^{4}He (^{6}He/He $\approx$ 0.003) both of which are available as beam nuclei for calibrations, and iv) the high detection efficiency for Z = 2 interactions. To date, preliminary results show the pattern of interaction of Z = 2 PFs from ^{56}Fe to be similar to those described above for $Z \geqslant 3$ PFs. Should this trend be sustained, the experiment will eliminate many of the uncertainties in previous experiments and will greatly clarify the interpretations of the results.

The rather surprising and, so far, baffling observations of PFs with anomalously short MFPs at Bevalac energies give urgent need of new experimental approaches and information. Future directions in such experiment must address questions pertaining to the lifetime of anomalons, production/reaction mechanisms, energy dependence, and, ultimately, masses and decay mechanisms. The experiments will be difficult but certainly motivated by the provocative hints of what may be a new state of nuclear matter.

I want to thank W. Loveland, S. Fung, W. Zajc, and my colleagues in the LBL-NRC collaboration for their critical comments and contributions of data for this review. This work was supported by the Director, Office of Energy Research, Division of Nuclear Physics of the Office of High Energy and Nuclear Physics of the U.S. Department of Energy under Contract W-7405-ENG-48.

References

1) G.F. Chew, Comments Nucl. Part. 2 (1968) 107

2) G.F. Chew, "High Energy Heavy Ion Beams as Tests of Nuclear Democracy and as a Tool to Clarify Regge Asymptotic Behavior," LBL Internal Report, March 10, 1972 (unpublished)

3) G.F. Chew, "Large and Small Baryon Numbers in High Energy Collision Theory," LBL Internal Report, May 31, 1973 (unpublished)

4) A.M. Baldin, Erice School on Heavy Ion Interactions at High Energies, Erice, Italy (1979) 95

5) A.S. Goldhaber and H.H. Heckman, Ann. Rev. Nucl. Part. Sci. 28 (1978) 161

6) J. Benecke, T.T. Chou, C.N. Yang and E. Yen, Phys. Rev. 188 (1969) 2159

7) R.P. Feyman, Phys. Rev. Lett. 23 (1969) 1415

8) W.R. Frazer, L. Ingber, C.H. Mehta, C.H. Poon, D. Silverman, K. Stowe, P.D. Ting and H.J. Yesian, Rev. Mod. Phys. 44 (1972) 284

9) H. Boggild and T. Ferbel, Annu. Rev. Nucl. Sci. 24 (1974) 451

10) J.B. Cumming, P.E. Haustein, T.J. Ruth and G.J. Virtes, Phys. Rev. C17 (1978) 1632

11) J.B. Cumming, R.W. Stoenner and P.E. Haustein, Phys. Rev. C14 (1976) 1554

12) N.T. Porile, G.D. Cole and C.R. Rudy, Phys. Rev. C19 (1979) 2288

13) D.J. Morrissey, W. Loveland, M. de Saint Simon and G.T. Seaborg, Phys. Rev. C21 (1980) 1783

14) W. Loveland, D.J. Morrissey, K. Aleklett, G.T. Seaborg, S.B. Kaufman, E.P. Steinberg, B.D. Wilkens, J.B. Cumming, P.E. Haustein and H.C. Hseuh, Phys. Rev. C23 (1981) 253

15) S.B. Kaufman, E.P. Steinberg, B.D. Wilkins and D.J. Henderson, Phys. Rev. C22 (1980) 1897

16) W. Loveland, Cheng Luo, P.L. McGaughey, D.J. Morrissey and G.T. Seaborg, Phys. Rev. C (in press); also Lawrence Berkeley Laboratory Report LBL-11658 (1980) 38 p.

17) L. Winsberg, Nucl. Instrum. Methods 150 (1978) 233

18) S.B. Kaufman, E.P. Steinberg and M.W. Weisfield, Phys. Rev. C18 (1978) 1349

19) N. Masuda and F. Uchiyama, Phys. Rev. C15 (1977) 1598

20) G.K. Gelbke, C. Olmer, M. Buenerd, D.L. Hendrie, J. Mahoney, M.C. Mermaz and D.K. Scott, Phys. Rep. 42 (1978) 312

21) N.T. Porile, Phys. Rev. 120 (1960) 572

22) A. Sandoval, H.H. Gutbrod, W.G. Meyer, R. Stock, Ch. Lukner, A.M. Poskanzer, J. Gosset, J.-C. Jourdain, C.H. King, G. King, Nguyen Van Sen, G.D. Westfall and K.L. Wolf, Phys. Rev. C21 (1980) 1321

23) K.B. Bhalla, M. Chaudhry, S. Lokanathan, R.K. Grover, I.K. Daftari, L.K. Mangotra, N.K. Rao, S. Garpman and I. Otterlund, "Relativistic α-particles emitted in Fe-emulsion interactions at 1.7 A GeV," Cosmic and Subatomic Physics Report LUIP8101, Lund University (1981) 23 p.

24) G. Cocconi, Phys. Lett. 49B (1974) 459

25) G.I. Kopylov, Phys. Lett. 50B (1974) 472

26) G.I. Kopylov and M.I. Podgoretsky, Yad. Fiz. 18 (1973) 656 [Sov. J. Nucl. Phys. 18 (1974) 336]

27) R. Hanbury-Brown and R.Q. Twiss, Nature 178 (1956) 1046

28) F.B. Yano and S.E. Koonin, Phys. Lett. 78B (1978) 556

29) S.Y. Fung, W. Gorn, G.P. Kiernan, J.J. Lu, Y.T. Oh and R.T. Poe Phys. Rev. Lett. 41 (1978) 1592

30) J.J. Lu, D. Beavis, S.Y. Fung, W. Gorn, H. Huie, G.P. Kiernan, R.T. Poe and G. Van Dalen, Phys. Rev. Lett. 46 (1981) 898

31) C. Ezell, L.F. Gutay, A.T. Laasanen, F.T. Dao, P. Schübelin and F. Turkot, Phys. Rev. Lett. 38 (1977) 873

32) Aachen-Berlin-Bonn-CERN-Cracow-Heidelberg-Warsaw Collaboration, Nucl. Phys. B103 (1976) 198

33) M. Gyulassy and S.K. Kaufman, Phys. Rev. Lett. 40 (1978) 298

34) J. Gosset, J.I. Kapusta, and G.D. Westfall, Phys. Rev. C18 (1978) 844

35) J.A. Bistirlich, R.J. Bossingham, H.R. Bowman, C.W. Clawson, K.M. Crowe, K.A. Frankel, O. Hashimoto, J.G. Ingersoll, M. Koike, J.P. Kurck, C.J. Martoff, J.P. Miller, D. Murphy, J.O. Rasmussen, J.P. Sullivan, P. Truöl, E. Yoo and W.A. Zajc, Proceedings of the Hakone Seminar, Vol. 1 (1980) 393; also private communication, W.A. Zajc

36) E.M. Friedlander, R.W. Gimpel, H.H. Heckman, Y.J. Karant, B. Judek and E. Ganssauge, Phys. Rev. Lett. 45 (1980) 1084